CRYSTAL GROWTH & DESIGN

Article

Cite This: Cryst. Growth Des. 2019, 19, 5850−5857

pubs.acs.org/crystal

Computed X-ray Tomography Study of Carbonate Precipitation in Large Portland Cement Pores

Elvia Anabela Chavez Panduro,*[,†] Malin Torsæter,[‡] Kamila Gawel,[‡] Ruben Bjørge,[‡] Alain Gibaud,[§] Anne Bonnin,[∥] Christian M. Schlepütz,[∥] and Dag Werner Breiby[†,⊥]

[†]PoreLab, Department of Physics, Norwegian University of Science and Technology (NTNU), Høgskoleringen 5, 7491 Trondheim, Norway

[‡]SINTEF Industry, Trondheim, Norway

[§]LUNAM, IMMM, UMR 6283 CNRS, Université du Maine, Le Mans Cedex 09, France

[∥]Swiss Light Source, Paul Scherrer Institute, Villigen, Switzerland

[⊥]Department of Microsystems, University of South-Eastern Norway, Campus Vestfold, 3184 Borre, Norway

Supporting Information

ABSTRACT: Cement degradation caused by CO_2 exposure is an increasingly important environmental challenge that must be understood, for example, if former oil reservoirs are to be used for CO_2 storage. When exposed to CO_2-saturated brine, cement undergoes a chemically complex carbonation process that influences all the physicochemical properties of the cement. It is known that under favorable conditions, fractures and voids in cement can be occluded, or self-sealed, by precipitation of calcium carbonate. Here, we report a detailed X-ray microcomputed tomography (μ-CT) study on the carbonation of gas pores (macropores) of diameter ∼1 mm in cement. Specifically, cured class G Portland cement with sub-millimeter spherical disconnected macropores was exposed to CO_2-saturated brine at high pressure (280 bar) and high temperature (90 °C) for 1 week. High-resolution synchrotron-based μ-CT enabled visualizing the morphology of the precipitates inside the macropores within both unreacted and carbonated regions. Quantitative analysis of the type and amount of material deposited in the macropores during carbonation suggests that the filling of the disconnected macropores involves transport of calcium ions from the cement bulk to the macropore interior. A detailed model describing the chemical processes involved is provided. The present study gives a deeper understanding of cement carbonation by literally shedding light on the complex precipitate structures within the macropores.

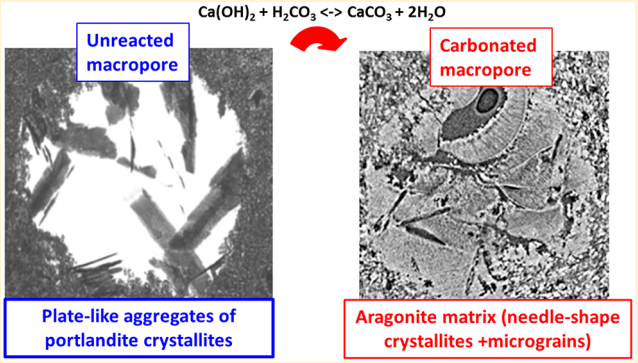

1. INTRODUCTION

Portland cement is a widely used construction material, and with the ongoing CO_2 climate crisis, understanding the interactions between cement and CO_2 is a topic of huge environmental importance. For example, Portland cement is currently used in well construction to isolate the annular space between the casing and drilled rock and to permanently close off the wellbore after it has finished its productive life. Despite its common use, cement is expected to be the well barrier element that most commonly fails and causes leakages.[1] Cement shrinks during solidification, it is brittle and prone to tensile cracking,[1] and its bonding strength to steel casings and rock formations is questionable.[2,3] The need for better understanding cement and its response to CO_2 under various conditions is frequently brought up in both industrial and scientific fora.[4]

Cement contains several types of pores or voids that have an important influence on its physicochemical properties. Mehta and Monteiro classified the types of pores as follows: gel pores have diameters of 15−20 Å, capillary pores range from 10 to 50 nm, and air (gas) pores are usually in the range between 0.05 mm and 2 mm.[1] The gel pores and capillary pores are commonly referred to in the literature as *micropores* and *mesopores*, respectively. The pores with a diameter larger than 50 nm are called macropores.[1] Whereas capillary pores are irregular in shape, gas pores are usually spherical.

The formation of the gas pores is caused by the entrapment of gas within the cement slurry during setting and hardening. In wells, such a gas entrapment may be a result of gas intrusions when cementing wells that penetrate into high-pressure reservoirs. Thus, it is likely that cement hardened at downhole conditions will contain natural gas bubbles.[5,6] Lile et al.[7] have shown that wellbore cement when cured in contact with gas

Received: July 3, 2019
Revised: August 20, 2019
Published: September 5, 2019

DOI: 10.1021/acs.cgd.9b00864
Cryst. Growth Des. 2019, 19, 5850−5857

(CH_4) may possess bubbles (spherical pores) of comparable pore size as the air bubbles in the cement slurry cured at low pressure. According to these authors, the reason why the bubbles form is dissolution of gas in the slurry and subsequent gas liberation due to pressure reduction during cement hydration. Gawel et al. have also observed macropores of different morphology in a CO_2 well plug cement cured at downhole conditions;[5] however, the origin of this porosity is unknown. These imperfections act as stress concentrators and decrease the mechanical stability of the cement. Moreover, cement is a brittle material, and the presence of macropores may promote microcracking.[2] Thus, macropores might affect the cement integrity even if they are not connected.

In recent papers, we have demonstrated that small cavities or cracks ("confined areas") in cement are particularly prone to be sealed when flowing CO_2-brine through connected channels in cement.[8,9] This phenomenon is caused by the precipitation of calcium carbonate (CC) within the free volume of the channels, as first reported by Liteanu et al.[10] Whether the channel gets healed or not depends on the residence time[11,12] (and thus the pH) of the fluid in the channel. Even if fractures develop from macropores, these defects may be sealed by CO_2 exposure as long as they do not constitute a continuous leakage path which would support reactant transport and thus faster degradation.[12] To better understand the carbonation and self-sealing phenomena in cement, it is essential to investigate in more detail the diffusion-driven reactions taking place inside non-connected isolated pores.

Although the chemical processes caused by exposure of cement to CO_2 are known and relatively well described in the literature,[11,13−16] the detailed physicochemical mechanisms of carbonation of macropores call for further investigations. In this paper, we present high-resolution microcomputed tomography (μ-CT) studies of the carbonation of isolated Portland cement macropores upon CO_2 saturated brine exposure at conditions of high pressure and high temperature. The high contrast and resolution of synchrotron-based μ-CT imaging made it possible to study directly and nondestructively the morphology and chemistry of material deposits inside macropores within both carbonated and unreacted regions of the cement samples, providing novel insight into the carbonation process of crystals of portlandite inside isolated gas pores in cement.

2. MATERIALS AND METHODS

2.1. Sample Preparation. A block of cement was prepared using ordinary Portland G cement (High Sulfate Resistant Well cement, Norcem Brevik) blended according to the API recommended practice[17] with a water/cement weight ratio of 0.44. The cement slurry was poured into a large cylindrical mold (diameter 90 mm and length 100 mm) and cured at 15 bar pressure supplied by nitrogen for 7 days in a pressure cell. This relatively low curing pressure compared to the downhole conditions was chosen in order to prevent gas compaction and maintain the macropores in the sub-millimeter range. As the spherical voids arise from trapped gas bubbles inside the cement, their diameter is strongly dependent upon the curing pressure. The cylindrical cores of diameter 20 mm used for the CO_2 exposure were cored out from the large cement block.

The cured core samples were exposed to CO_2-saturated brine in a pressure cell of diameter 90 mm kept inside a furnace. Before exposure, the cores were submerged in 1 wt % NaCl solution inside a vacuum chamber connected to a water aspirator for more than 1 day, to enable brine absorption in the cement. The cores were then transferred to the pressure cell, and fresh brine (1 wt % NaCl) was added up to approximately 10 mm above the samples. The estimated amount of fresh brine was 250 cm^3, and the volume ratio solid/brine was around 12. CO_2 gas was supplied from the top of the cell. The cell was gradually pressurized by pumping CO_2 up to 280 bar during 6−8 h. During the 1 week of CO_2 exposure, the temperature was kept at 90 °C and the CO_2 pressure was maintained at 280 bar—at these conditions the CO_2 is in a supercritical state. At the end of the exposure, the pressure and temperature were decreased gradually over 6−8 h to prevent the sample from cracking. After the exposure, the cement was stored in sealed containers. For this study, two core samples cured and exposed to CO_2 under the same conditions have been used, referred to as Core A and Core B. The samples for high-resolution tomography were obtained by cutting prism-shaped pieces of approximate size $1 \times 1 \times 4$ mm^3 from selected regions of the carbonated cement. All cutting was done using a diamond blade wetted with anhydrous ethanol.

2.2. Sample Characterization. In-house X-ray microcomputed tomography (μ-CT) was used to examine the physical changes in the cement core samples after exposure to CO_2. The μ-CT images were collected with the attenuation-contrast Nikon XTH 225 scanner at the Department of Physics, NTNU. The samples were exposed to a polychromatic cone-shaped beam from a tungsten target, using an acceleration voltage of 114 keV and a tube current of 160 μA, with an exposure time of 1000 ms per projection. A total of 3142 projections evenly distributed over 360° were collected. Brighter grayscales correspond to higher X-ray absorption, and they can be correlated to atomic number and density of the materials being imaged. Three-dimensional reconstructions were done using the CT-Agent program supplied by Nikon, here giving a resolution of around 15 μm.

High-resolution μ-CT was obtained at the TOMCAT beamline at the Swiss Light Source, Paul Scherrer Institute. The measurements were done with a monochromatic beam of energy 20 keV. The 1501 projection images over a sample rotation angle of 180° were collected using a 20 μm thick LuAG:Ce scintillator and a CCD detector, giving a field of view of 1.7×1.4 mm^2, an effective pixel size of 0.65×0.65 μm^2, exposure time 250 ms, and a distance from the sample to the detector of 72 mm. At this sample−detector distance, the attenuation contrast is enhanced by propagation phase contrast.[18] For the reconstructions of the phase-contrast 2D projections, the TOMCAT reconstruction pipeline[19−21] was used. The resolution of the reconstructed images is close to 1 μm. Segmentation and visualization of the 3D high-resolution synchrotron images were done using VGStudio (Volume Graphics GmbH). Segmentation and volume calculations of the pores and the precipitates were done by applying simple thresholding. The error bars were estimated from the different grayscale values used during the segmentation, and the range of the values was chosen by visualization of the maximum and minimum segmented area that could represent the object.

The X-ray diffraction (XRD) measurements were carried out using Cu K_α radiation (wavelength of 1.54 Å) on a Panalytical Empyrean working at 40 kV and 30 mA. The beam from the copper anode was monochromatized and collimated by reflection on a multilayer mirror. The full width at half-maximum of the direct beam was 0.06° with a peak intensity of about 50×10^6 counts/s. The powder samples for XRD measurements were obtained by mechanically extracting the precipitate from the macropores, using a lab spatula. As the amount of powder was small, it was deposited on a miscut silicon sample holder, which gives a low background at wide scattering angles. The relative amounts of crystalline phases were estimated using the MAUD program[22] based on Rietveld refinement.

Scanning electron microscopy (SEM) was performed using Hitachi S-3400N and Hitachi SU-6600 microscopes in the backscattered electron (BSE) mode. Epoxy was used to mechanically stabilize the sample before cutting and polishing the SEM samples. A thin layer of 15 nm of Pd and Pt was deposited on the specimen to reduce sample charging.

3. RESULTS

3.1. Carbonation of Bulk Cement. A 20 mm cylindrical Portland cement core was exposed to CO_2 saturated brine at 90 °C and 280 bar for 1 week, as described in section 2.2. Figure 1a,b shows a 3D perspective and a cross-section through the

DOI: 10.1021/acs.cgd.9b00864
Cryst. Growth Des. 2019, 19, 5850−5857

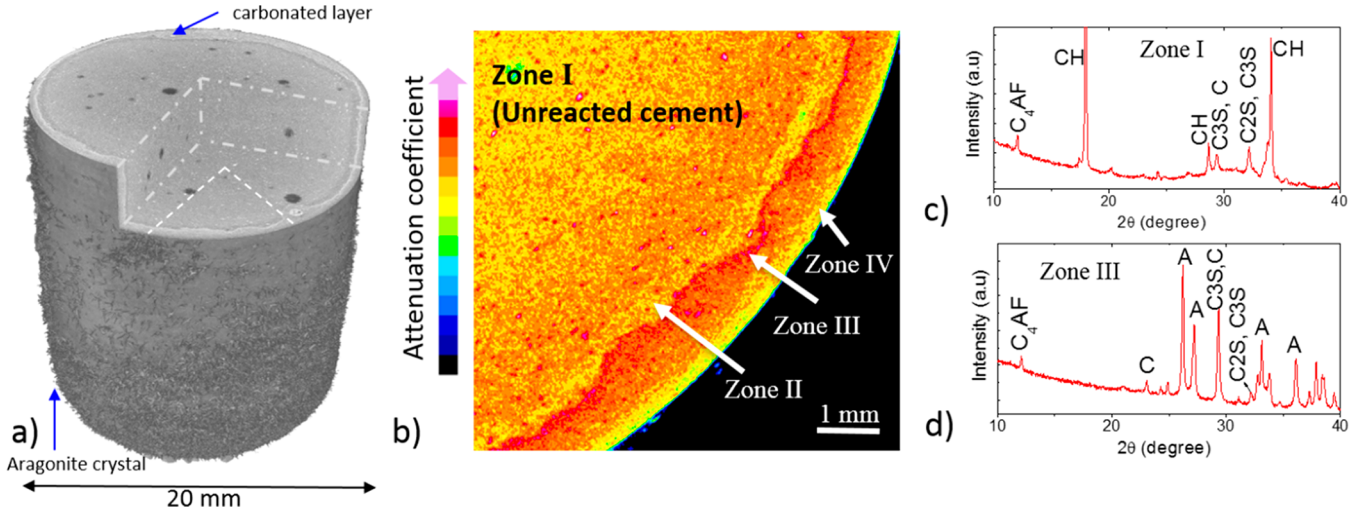

Figure 1. Portland cement (core A) exposed to CO_2 saturated brine for 1 week at 90 °C and 280 bar. (a) Perspective cut-away view of the home laboratory μ-CT reconstruction. (b) False-colored μ-CT cross-section with clearly observable regions. (c, d) X-ray diffraction patterns of material retrieved from Zones I and III, respectively, with peaks assigned to crystalline phases: portlandite (CH); dicalcium silicate (C_2S); tricalcium silicate (C_3S); tetracalcium alumino ferrite (C_4AF); aragonite (A); calcite (C). The intensity gradient (lighter moving inward) in Zone I is a CT reconstruction artifact.

CO_2-exposed core. An approximately 1.5 mm thick carbonated layer is visible as a bright rim around the core; see Figure 1a. Figure 1c presents an XRD pattern collected from the powder extracted from the unreacted bulk cement, confirming that the main crystalline hydration product present in the cement bulk is portlandite $Ca(OH)_2$ (CH in cement chemist notation). Other crystalline phases identified by XRD are nonhydrated cement components, specifically dicalcium silicate (C_2S), tricalcium silicate (C_3S), and tetracalcium aluminoferrite (C_4AF). In addition, the presence of an amorphous phase was manifested in the XRD patterns in the form of a broad diffraction peak seen in the 2θ range between approximately 25 and 37 degrees, cf. Figures 1c and S2b. The amorphous phase is identified in the literature as calcium silicate hydrate (CSH), typically constituting ~70 wt % of hydrated cement.[14,23] Both the crystalline CH and the amorphous CSH phase are susceptible to carbonation.[13]

When hydrated cement is submerged in CO_2 saturated brine solution, the carbonic acid diffuses into the cement bulk, referred to as Zone I, cf. Figure 1b.[13] The acidic brine first dissolves the CH in the cement leaving a CH depleted layer,[13] denoted Zone II. At the high pH present in cement, the dissolved calcium ions precipitate in the form of calcium carbonate in the carbonated region (Zone III). The observed line of high attenuation separating Zones II and III is the carbonation front. Immediately behind the carbonation front, within Zone III, the concentration of CC is the highest, as indicated by the high X-ray attenuation coefficient values (red color in Figure 1b). The amount of CC decreases gradually toward the sample edge. The thin layer of Zone IV outside the carbonated region (yellow to green color in Figure 1b) is according to the literature almost calcium-free and consists mainly of amorphous silica.[12−14,24−26]

The XRD pattern obtained with material from Zone III, cf. Figure 1d, shows that in this region, the vastly dominating CC polymorph is aragonite, in agreement with refs 27 and 28. The high relative abundance of aragonite is ascribed to the high-temperature conditions used during CO_2 exposure, corroborating observations reported by Ogino[29] for CC precipitating in the temperature range between 60 and 80 °C. In the unreacted region of Zone I, XRD indicated there is no aragonite, but some calcite, which it is reasonable to assume that originates from carbonation processes taking place at ambient conditions after the CO_2 exposure and before and after extracting the powder from the macropore for XRD measurement. The crystallites that can be discerned on the outer surface of the cement cores (see also Figure 1a) were identified by XRD as aragonite, most likely precipitated during the depressurization of the cell.

3.2. Carbonation of Macropores. The above-described carbonation processes in the cement bulk were accompanied by morphological changes within the macropores. The free (void) volumes of the macropores were strongly reduced after the carbonation front had passed. Figure 2 shows the volume

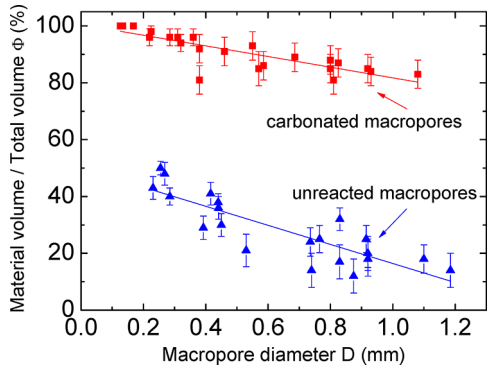

Figure 2. Volume filling fraction Φ of precipitates in macropores (core B), plotted as a function of the macropore diameter D. Note the trend of decreasing Φ with increasing D and the fact that the macropores in the unreacted cement (blue triangles) contain less than half the amount of material found in the carbonated cement pores (red squares).

fraction Φ of the macropores filled by precipitated minerals after the one-week exposure, plotted as a function of their diameter D, for both unreacted and carbonated regions. The filling fraction Φ decreased with increasing D. By fitting, we obtain $\Phi^0(\%) = -33D + 50$ for the unreacted macropores, and $\Phi^{carb}(\%) = -18D + 100$ (D in mm) for the carbonated macropores. In the carbonated region (Zone III), the volume fraction occupied by

DOI: 10.1021/acs.cgd.9b00864
Cryst. Growth Des. 2019, 19, 5850−5857

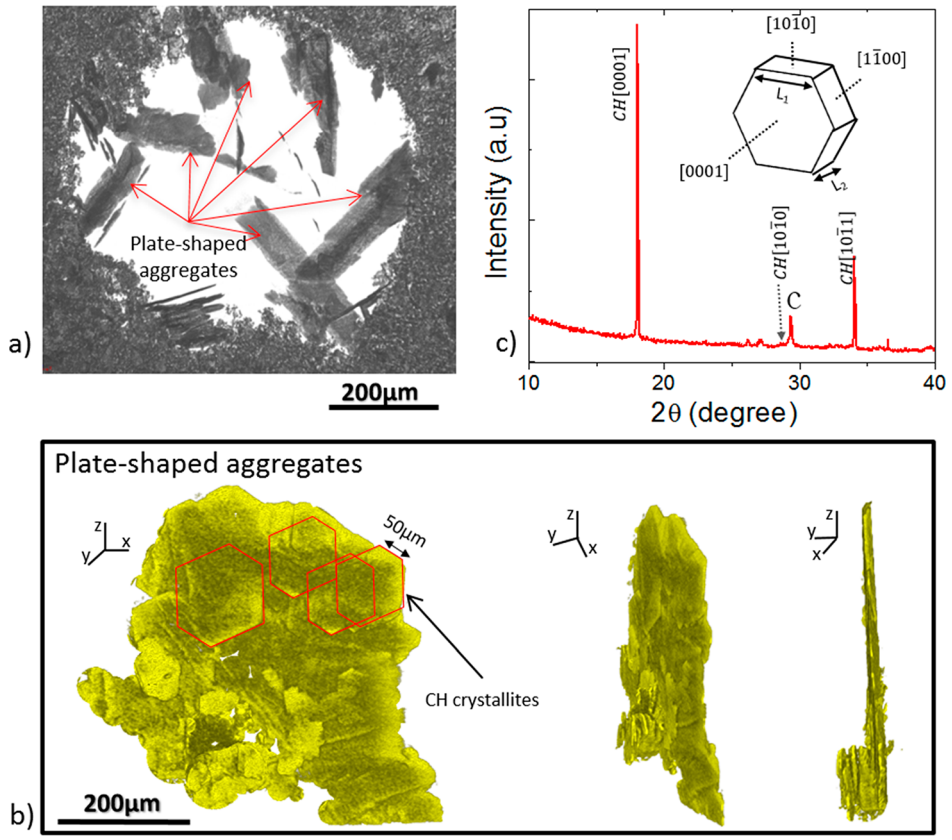

Figure 3. Macropore in the unreacted cement, Zone I (sample obtained from Core B). (a) High-resolution μ-CT cross-section. (b) Magnified view of a single plate-shaped aggregate at different viewing angles. (c) XRD pattern of material retrieved from the unreacted macropore confirming the presence of mainly CH. The inset depicts the hexagonal-prism shape of the CH crystallite. CH: calcium hydroxide, C: calcite.

precipitated material was on average more than twice higher than in the unreacted region (Zone I).

The reduction of the void volume of the macropores ("self-sealing") upon exposure to supercritical CO_2 is caused by precipitation of poorly water-soluble calcium carbonate (solubility of CC in water at 25 °C is 0.013 g/L)[30] within the available pore matrix.[31,32] The smallest resolved pores of a diameter just below ~0.2 mm were found to be entirely filled with CC. This observation suggests that after a certain exposure time, in the current case 1 week, there is a threshold volume up to which closed macropores are entirely filled with CC, and above which some free volume will be present in the pores. This threshold value would likely depend on the cement composition, but also the curing and carbonation conditions. We consider it likely that also larger pores would tend to fill completely with longer exposure times.

3.3. High-Resolution Imaging of Precipitates in Macropores. In order to gain a better understanding of the morphology and carbonation processes taking place in the macropores, smaller physically cut cement samples containing macropores were subjected to high-resolution synchrotron μ-CT. Results obtained for a selected macropore in the unreacted region (Zone I) of the cement specimen are collected in Figure 3. High-resolution μ-CT shows that the macropore was filled with subhedral plate-shaped aggregates of hexagonal crystals as reported by Bache et al. using optical microscopy.[33] When Portland cement is hydrated, CH, CSH, and hexacalcium aluminate trisulfate hydrate (ettringite) are typically formed.[34] X-ray powder diffraction data obtained on material extracted from a macropore in unreacted cement showed sharp peaks corresponding to the presence of calcium hydroxide, but no amorphous peak, suggesting that if CSH were present in the pore, it were in negligible quantities only. The observed hexagonal plate-shaped of the crystallites provided by μ-CT is also consistent with the mineral present inside the macropore being portlandite (space group 156, $P3m$). The μ-CT image shows crystallites aggregates, supposedly coaligned along their [0001] faces as judged by their external shape. Typical dimensions of the hexagonal crystallites in the present case were L_1 = 50 μm (length of the hexagon edge, see inset of Figure 3c) estimated by μ-CT, and L_2 = 1 μm (thickness) estimated by μ-CT and peak broadening in the XRD pattern. These precipitated CH crystallites were larger than the CH crystallites observed in the cement bulk (see Supporting Information S1), which is possibly a result of the larger available volume for growth in the macropores compared to the bulk cement.

Results obtained for a selected carbonated macropore are collected in Figure 4. When the CH-rich macropore got in contact with carbonated water diffusing through the cement matrix, carbonation took place. This process is based on the dissolution of calcium hydroxide and reaction between calcium ions with carbonate ions according to the equation: $Ca^{2+} + CO_3^{2-} \leftrightarrow CaCO_3$ (s). In order to analyze the mineralogical composition of material retrieved from the interior of carbonated macropores, X-ray powder diffraction was carried out, confirming the presence of CC as aragonite and calcite. The relative amount of aragonite was 90 wt % of the crystalline phases, as quantified by MAUD (Figure S2a).[22]

The very same carbonated macropore, imaged first with high-resolution μ-CT and later (after physical sectioning) by SEM, is

DOI: 10.1021/acs.cgd.9b00864
Cryst. Growth Des. 2019, 19, 5850−5857

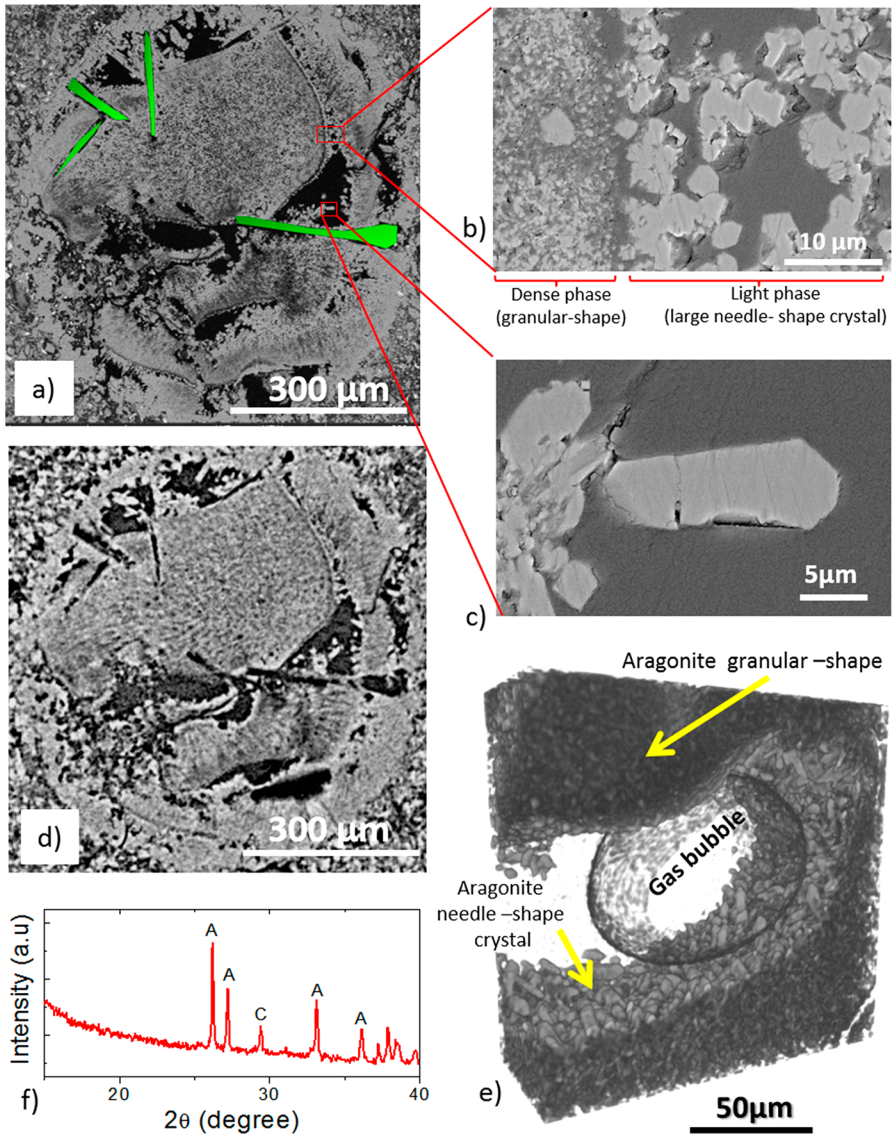

Figure 4. Macropores in carbonated cement, Zone III (sample from core B). (a) SEM-BSE micrograph of a physical cut through a macropore. Empty spaces after dissolved CH crystallites are highlighted in green (see also Figure S4). (b, c) SEM-BSE images of selected areas showing a denser and a lighter phase. (d) High-resolution μ-CT cross-section of the very same macropore as observed by SEM-BSE in (a). (e) High-resolution μ-CT perspective view of the interface between the granular and needle-shaped precipitates. A gas bubble is observed residing in the free volume of the carbonated macropore. (f) XRD pattern of material retrieved from the carbonated pore. C: calcite, A: aragonite.

shown in Figure 4. Gratifyingly, the corresponding cross-sections are in full agreement, as can be seen by comparing Figure 4a and d. The macropore is almost entirely filled by precipitated CC, apparently formed by several consecutive layers of precipitation in the direction of the fluid diffusion; see also Discussion and Supporting Information S3. As a part of these layered structures, two morphologies can be distinguished within the precipitate: (i) a dense low-porosity phase consisting of agglomerated aragonite micrograins of characteristic size around 1 μm, and (ii) a lighter, more porous phase of larger needle-shaped aragonite crystals of around 5−10 μm in length; see Figure 4b,c.

Interestingly, empty characteristic plate-shaped voids (appearing needle-shaped in the image cross-section), highlighted in green in Figure 4a, are observed in the CC precipitate. From their characteristic shape, and by comparison with the unreacted pores (see Figure 3a), these voids are understood to be the vacated volumes remaining after dissolved CH crystallites. The presence of these empty volumes strongly suggests that the precipitation of CC took place *before* all the CH crystals present in the macropore were dissolved. The "free volume" in the carbonated macropore was mainly filled by a liquid, but also up to five gas bubbles of similar diameter ~200 μm were observed within the liquid inside the macropore using synchrotron μ-CT; see Figure 4e for a selected example. The liquid inside the macropore must have been carbonated brine containing minerals dissolved from the cement matrix.

4. DISCUSSION

The carbonation process within the macropores was found to be different from the carbonation of the bulk cement. While the CH and CSH phases undergo carbonation in the cement bulk, inside the macropores only CH is available for carbonation reactions according to the presented XRD analysis. Only a small fraction of the macropore volume in unreacted cement was filled with CH, and the remaining volume was filled with air. This air-filled

DOI: 10.1021/acs.cgd.9b00864
Cryst. Growth Des. 2019, 19, 5850−5857

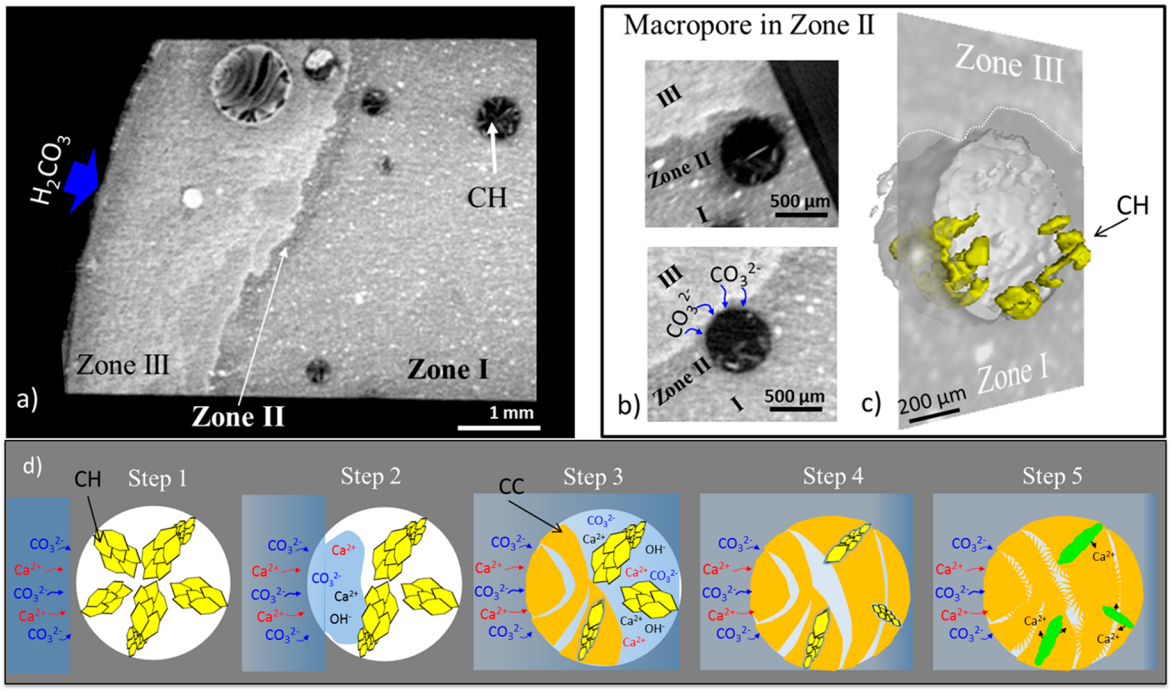

Figure 5. Schematic model and supporting observations of macropore carbonation. (a) CT cross-section of the partially carbonated Portland cement sample. While the macropores in the unreacted Zone I are filled with plate-shaped CH crystallites, the macropores in the carbonated Zone III are clogged with precipitated CC. (b) CT cross-sections of two isolated macropores from CH depleted Zone II. Note the absence of CH crystallites within the macropores on the side facing the carbonation front. (c) 3D perspective representation of the macropore in Zone II. (d) The carbonation process within the macropores can be described with the indicated steps detailed in the main text.

void macropore volume was available for precipitation of the carbonation product, i.e., calcium carbonate.

The qualitatively different appearance of the macropores in the unreacted (Zone I) and carbonated regions (Zone III), as well as at the interface (Zone II), is highlighted in Figure 5. Macropores within the carbonated region (Zone III) tend to be filled with CC and fluid, most likely water saturated with ions. Notably, some macropores located exactly at the carbonation front are seen to contain (i) CC crystals near the carbonated region, (ii) CH crystals in the unreacted region, and (iii) a partial volume depleted of CH. Whether all these three regions are present within the macropore depends on the advancement of the carbonation front.

The observed average volume of the material deposited within the carbonated macropores was much higher than the volume increase expected from the stoichiometric carbonation of the CH present in the unreacted macropores. The XRD measurement indicated that all the material present inside the unreacted macropores was crystalline CH. The volume increase associated with complete carbonation of CH can be estimated to be around 10 vol %. The macropores in the unreacted region were on average filled up to 30 vol % with CH, while macropores in the carbonated region were filled up to 90 vol % with CC. The high degree of pore filling suggests that the CC residing in the pores after carbonation originates from two disparate sources: (i) carbonated CH and (ii) additional CC that has diffused into the pore. This additional CC must originate from the surrounding cement as a reaction product between calcium ions diffusing into the macropore space from the cement bulk and carbonate ions diffusing along with the carbonation front.

Empty spaces after CH crystallite dissolution (highlighted in green in Figure 4a) were observed, strongly suggesting that the precipitation of CC took place *before* all the CH crystallites present in the macropore were dissolved. This can be understood by noting that dissolution of CH and precipitation of CC require different conditions. While CH dissolution will be supported by low pH and low calcium ion concentration in brine, precipitation of CC will be promoted at high pH conditions and a high concentration of calcium ions. Thus, these two parameters together determine whether dissolution or precipitation will occur at a given place and time. Dissolving CH is a source of OH^- ions as well as Ca^{2+} ions and may give a fast increase of pH and oversaturation of Ca^{2+}, resulting in precipitacion of CC. This fast increase of both pH and Ca^{2+} concentration may be the reason why the precipitation of CC took place before the dissolution of CH was completed. With the continued invasion of acidic brine, the pH decreases, promoting dissolution of the CH remaining in the macropore. Now, the acidic brine may interact with both CH and CC present in the pore space. However, the solubility of CH is higher compared to CC (2.5×10^{-2} mol/L for CH vs 1.3×10^{-4} mol/L for CC at standard conditions), and it is thus likely that dissolution of CH can take place before CC dissolution starts. The calcium ions released from the dissolving CH might have diffused away and deposited at other locations with conditions more favorable for CC precipitation. One possible location could be the interior of the pore. The presence of two different aragonite crystal deposition stages, giving micrograins and needle-shaped crystals, suggests that the precipitation was a two-stage process. Presumably, in the first stage, the formation of a large number of nuclei in oversaturated brine led to precipitation of microsized granular crystals inside the pore. In the second stage, slow growth of crystallites, most likely from brine wetting the microcrystalline matrix, took place resulting in the formation of euhedral needle-shaped aragonite crystals. It is likely that these needle-like crystallites are carbonation products of CH

DOI: 10.1021/acs.cgd.9b00864
Cryst. Growth Des. 2019, 19, 5850−5857

crystallites remaining from the first precipitation stage. Another possibility is that the ions were transported deeper into the cement, i.e., toward the new carbonation zone. These hypotheses require experimental validation.

Model for Macropore Carbonation. The analysis of the μ-CT images, SEM, and powder XRD data support the proposed macropore carbonation mechanism depicted graphically in Figure 5d. In step 1, the carbonated water containing carbonic acid diffuses inward through the cement matrix and eventually reaches the macropore edge. During step 2, the liquid containing dissociated acid first dissolves the CH platelets at the macropore perimeter facing the incoming carbonation front. Step 3, when the concentration of the dissolved calcium ions in the carbonated brine in a given macropore exceeds the saturation threshold, CC is precipitated. Step 4, deposition of CC in the remaining volume, consuming Ca^{2+} ions from the cement bulk (red) and Ca^{2+} ions from inside the macropore (black). The oversaturation and subsequent carbonate precipitation take place before all CH crystals present in the macropore have dissolved. In step 5, with the continued supply of brine, the pH is reduced, thereby dissolving the remaining CH crystallites leaving empty volumes (highlighted in green in Figure 5d) and Ca^{2+} ions are precipitating into the CC matrix or being transported more deeply into the cement to contribute to the advancing carbonation front. Also, calcium ions diffusing in from the cement bulk can be deposited in the macropore, resulting in the observed filling ratio Φ of CC in the macropores being much larger than would be expected from the carbonation of CH residing in the macropore volume only. Thus, the deposition of the calcium ions released from the cement bulk into the macropore volume contributes to sealing the macropores. It should be noted that while the outlined model process is supported by all the experimental data available, somewhat modified mechanisms can be envisioned. Notably, depending on the exact local physicochemical conditions, the pH and concentration conditions might even be oscillating, possibly explaining the successive layer deposition. The exact timing of the CH crystallite dissolution with respect to the final deposition of CC could be an interesting topic for further studies.

CONCLUSIONS

In this article, we have presented a comprehensive CT, SEM, and XRD study of cement carbonation upon exposure to CO_2-saturated brine at downhole conditions. In particular, we have demonstrated experimentally that the macropores, or gas pores, in cement get filled with CC when the carbonation front passes. The differences between the carbonation processes occurring in the bulk cement compared to the macropores have been emphasized, and we describe in detail the precipitation in macropores. Our model for the sealing process can be divided into the following stages: (1) diffusion of carbonated water through the cement matrix to the macropore, (2) local dissolution of CH, (3) oversaturation with Ca^{2+} inside macropore and precipitation of CC, (4) deposition of CC in the remaining volume, and (5) pH decreases due to the continued invasion of brine, dissolving the remaining CH. Aragonite is suggested to precipitate in two stages leading to two morphologically different deposits (micrograins and elongated needles growing at the outskirts of the grainy aggregates). We observed an increase in the filling ratio of the macropores after carbonation, suggesting that calcium ions released from the surrounding cement bulk are preferentially precipitated in the macropores. While giving new insights into the detailed carbonation mechanisms of cement exposed to CO_2, our study also reveals the need for understanding quantitatively the correlation between the cement compositions, curing conditions, and self-sealing capabilities of microsized gas inclusions in cement.

ASSOCIATED CONTENT

Supporting Information

The Supporting Information is available free of charge on the ACS Publications website at DOI: 10.1021/acs.cgd.9b00864.

Information regarding pore density in the cement, additional CT cross-section images of the cement showing the empty spaces after CH crystallite dissolution, and crystal precipitation fronts in carbonated macropores (PDF)

Movies showing cross-section slice across the unreacted and carbonated macropore (AVI1, AVI2)

AUTHOR INFORMATION

Corresponding Author

*E-mail: elviachavezp@gmail.com.

ORCID

Elvia Anabela Chavez Panduro: 0000-0003-3732-356X

Christian M. Schlepütz: 0000-0002-0485-2708

Notes

The authors declare no competing financial interest.

ACKNOWLEDGMENTS

This study has been partially funded by the projects "Closing the gaps in CO_2 well plugging" funded by the Research Council of Norway (243765/E20). The project is administered as an integrated part of the BIGCCS Centre funded by Gassco, Shell, Statoil, Total, Engie, and the Research Council of Norway (193816/S60). We acknowledge the Paul Scherrer Institut, Villigen, Switzerland, for provision of synchrotron radiation beamtime at the TOMCAT beamline X02DA of the Swiss Light Source. D.W.B. thanks the Research Council of Norway through its Centres of Excellence Funding Scheme (Project Number 262644) and the FRINATEK Program (Project Number 275182).

REFERENCES

(1) Mehta, P. K.; Monteiro, P. J. M. *Concrete Microstructure, Properties and Materials*; McGraw-Hill: USA, 2006.

(2) Lavrov, A.; Todorovic, J.; Torsæter, M. Impact of voids on mechanical stability of well cement. *Energy Procedia* **2016**, *86*, 401−410.

(3) Torsæter, M.; Todorovic, J.; Lavrov, A. Structure and debonding at cement − steel and cement − rock interfaces: Effect of geometry and materials. *Constr. Build. Mater.* **2015**, *96*, 164−171.

(4) Stripple, H.; Ljungkrantz, C.; Gustafsson, T.; Andersson, R. *CO_2 Uptake in Cement-Containing Products*; published by Swedish Cement and Concrete Research Institute (CBI), 2018.

(5) Gawel, K.; Todorovic, J.; Liebscher, A.; Wiese, B.; Opedal, N. Study of materials retrieved from a Ketzin CO_2 monitoring well. *Energy Procedia* **2017**, *114* (1876), 5799−5815.

(6) Kuzielova, E.; Zemlicka, M.; Masilko, J.; Palou, M. T. Geothermics Pore structure development of blended G-oil well cement submitted to hydrothermal curing conditions. *Geothermics* **2017**, *68*, 86−93.

(7) Lile, O. B.; Justnes, H.; Skalle, P.; Backe, K. R.; Sveen, J. Dissolved gas as a problem in oil well cements. *Adv. Cem. Res.* **1996**, *8* (32), 137−142.

(8) Panduro, E. A. C.; Torsæter, M.; Gawel, K.; Bjørge, R.; Gibaud, A.; Yang, Y.; Bruns, S.; Zheng, Y.; Sørensen, H. O.; Breiby, D. W. In-Situ X-

DOI: 10.1021/acs.cgd.9b00864
Cryst. Growth Des. 2019, 19, 5850−5857

ray Tomography Study of Cement Exposed to CO_2 Saturated Brine. *Environ. Sci. Technol.* **2017**, *51*, 9344−9351.
(9) Chavez Panduro, E. A.; Torsæter, M.; Gawel, K.; Bjørge, R.; Gibaud, A.; Yang, Y.; Sørensen, H. O.; Frykman, P.; Kjøller, C.; Breiby, D. W. Closing of micro-cavities in well cement upon exposure to CO_2 brine. *Energy Procedia* **2017**, *114*, 5100−5108.
(10) Liteanu, E.; Spiers, C. J.; Peach, C. J. Failure behaviour wellbore cement in the presence of water and supercritical CO_2. *Energy Procedia* **2009**, *1* (1), 3553−3560.
(11) Brunet, J.-P. L.; Li, L.; Karpyn, Z. T.; Huerta, N. J. Fracture opening or self-sealing Critical residence time as a unifying parameter for cement−CO_2−brine interactions. *Int. J. Greenhouse Gas Control* **2016**, *47*, 25−37.
(12) Carroll, S.; Carey, J. W.; Dzombak, D.; Huerta, N. J.; Li, L.; Richard, T.; Um, W.; Walsh, S. D. C.; Zhang, L. Review: Role of chemistry, mechanics, and transport on well integrity in CO2 storage environments. *Int. J. Greenhouse Gas Control* **2016**, *49*, 149−160.
(13) Kutchko, B. G.; Strazisar, B. R.; Dzombak, D. A.; Lowry, G. V.; Thaulow, N. Degradation of well cement by CO2 under geological sequestration conditions. *Environ. Sci. Technol.* **2007**, *41* (13), 4787−4792.
(14) Kutchko, B. G.; Strazisar, B. R.; Lowry, G. V.; Dzombak, D. A.; Thaulow, N. Rate of CO2 Attack on Hydrated Class H Well Cement under Geologic Sequestration Conditions. *Environ. Sci. Technol.* **2008**, *42*, 6237−6242.
(15) Duguid, A.; Radonjic, M.; Scherer, G. Degradation of Well Cements Exposed to Carbonated Brine. In *Proceeding of Fourth Annual Conference on Carbon Capture and Sequestration*; DOEINETL, 2005.
(16) Liteanu, E.; Spiers, C. J. Fracture healing and transport properties of wellbore cement in the presence of supercritical CO_2. *Chem. Geol.* **2011**, *281*, 195−210.
(17) Standard 10 B-2, American Petroleum Institute.
(18) Paganin, D.; Mayo, S. C.; Gureyev, T. E.; Miller, P. R.; Wilkins, S. W. Simultaneous phase and amplitude extraction from a single defocused image of a homogeneous object. *J. Microsc.* **2002**, *206* (1), 33−40.
(19) Weitkamp, T.; Haas, D.; Wegrzynek, D.; Rack, A. ANKAphase: Software for single-distance phase retrieval from inline X-ray phase-contrast radiographs. *J. Synchrotron Radiat.* **2011**, *18* (4), 617−629.
(20) Marone, F.; Stampanoni, M. Regridding reconstruction algorithm for real-time tomographic imaging. *J. Synchrotron Radiat.* **2012**, *19*, 1029−1037.
(21) Hintermuller, C.; Marone, F.; Isenegger, A.; Stampanoni, M. Image processing pipeline for synchrotron-radiation-based tomographic microscopy. *J. Synchrotron Radiat.* **2010**, *17*, 550−559.
(22) Lutterotti, L. Total pattern fitting for the combined size-strain-stress-texture determination in thin film diffraction. *Nucl. Instrum. Methods Phys. Res., Sect. B* **2010**, *268*, 334−340.
(23) Zhang, M.; Bachu, S. Review of integrity of existing wells in relation to CO_2 geological storage: What do we know? *Int. J. Greenhouse Gas Control* **2011**, *5* (4), 826−840.
(24) Kutchko, B. G.; Strazisar, B. R.; Huerta, N.; Lowry, G. V.; Dzombak, D. A.; Thaulow, N. CO_2 reaction with hydrated class H well cement under geologic sequestration conditions: Effects of flyash admixtures. *Environ. Sci. Technol.* **2009**, *43* (10), 3947−3952.
(25) Duguid, A.; Scherer, G. W. Degradation of oilwell cement due to exposure to carbonated brine. *Int. J. Greenhouse Gas Control* **2010**, *4* (3), 546−560.
(26) Huerta, N. J.; Hesse, M. A.; Bryant, S. L.; Strazisar, B. R.; Lopano, C. L. Experimental evidence for self-limiting reactive flow through a fractured cement core: Implications for time-dependent wellbore leakage. *Environ. Sci. Technol.* **2013**, *47* (1), 269−275.
(27) Declet, A.; Reyes, E.; Suárez, O. Calcium Carbonate Precipitation: a Review of the Carbonate Crystallization Process and Applications in Bioinspired Composites. *Rev. Adv. Mater. Sci.* **2016**, *44*, 87−107.
(28) de Leeuw, N. H.; Parker, S. C. Surface Structure and Morphology of Calcium Carbonate Polymorphs Calcite, Aragonite, and Vaterite: An Atomistic Approach. *J. Phys. Chem. B* **1998**, *102* (16), 2914−2922.
(29) Ogino, T.; Suzuki, T.; Sawada, K. The formation and transformation mechanisme of calcium carbonate in water. *Geochim. Cosmochim. Acta* **1987**, *51*, 2757−2767.
(30) Ayward, G. H.; Findlay, T. J. V. *SI Chemical Data*, 4th ed.; Wiley, 1999.
(31) Bachu, S.; Bennion, D. B. Experimental assessment of brine and/or CO_2 leakage through well cements at reservoir conditions. *Int. J. Greenhouse Gas Control* **2009**, *3* (4), 494−501.
(32) Garcia-Gonzalez, C. A.; el Grouh, N.; Hidalgo, A.; Fraile, J.; Lopez-Periago, A. M.; Andrade, C.; Domingo, C. New insights on the use of supercritical carbon dioxide for the accelerated carbonation of cement pastes. *J. Supercrit. Fluids* **2008**, *43* (3), 500−509.
(33) Bache, H. H.; Idorn, G. M.; Nepper-Christensen, P.; Nielsen, J. Morphology of Calcium Hydroxide in Cement Paste. *Highway Research Board Special Report* **1966**, 154−174.
(34) Taylor, H. F. W. *Cement Chemistry*, 1997. DOI: 10.1680/cc.25929

DOI: 10.1021/acs.cgd.9b00864
Cryst. Growth Des. 2019, 19, 5850−5857